

Magnesium *K*-edge XANES spectroscopy of geological standards

Toshihiro Yoshimura,^{a,*‡} Yusuke Tamenori,^b Nozomu Iwasaki,^c
Hiroshi Hasegawa,^d Atsushi Suzuki^e and Hodaka Kawahata^a

^aAtmosphere and Ocean Research Institute, The University of Tokyo, 5-1-5 Kashiwanoha, Kashiwa, Chiba 277-8564, Japan, ^bJapan Synchrotron Radiation Research Institute/SPring-8, 1-1-1 Kouto, Sayo 679-5198, Japan, ^cDepartment of Environment Systems, Rissho University, Magechi 1700, Kumagaya 360-0194, Japan, ^dInstitute of Science and Engineering, Kanazawa University, Kakuma, Kanazawa, Ishikawa 920-1192, Japan, and ^eGeological Survey of Japan, National Institute of Advanced Industrial Science and Technology (AIST), Tsukuba Central 7, 1-1-1 Higashi, Tsukuba, Ibaraki 305-8567, Japan. E-mail: yoshimura@aori.u-tokyo.ac.jp

Magnesium *K*-edge X-ray absorption near-edge structure (XANES) spectra have been investigated to develop a systematic understanding of a suite of Mg-bearing geological materials such as silicate and carbonate minerals, sediments, rocks and chemical reagents. For the model compounds the Mg XANES was found to vary widely between compounds and to provide a fingerprint for the form of Mg involved in geologic materials. The energy positions and resonance features obtained from these spectra can be used to specify the dominant molecular host site of Mg, thus shedding light on Mg partitioning and isotope fractionation in geologic materials and providing a valuable complement to existing knowledge of Mg geochemistry.

Keywords: magnesium; XANES; geologic material; SPring-8.

1. Introduction

Magnesium geochemistry plays a central role in a variety of geochemical and biochemical processes. The characteristic variations of Mg partitioning in geologic materials have been used in a variety of contexts. In the field of paleoceanography, Mg/Ca ratios of biogenic CaCO₃ have been used to estimate past changes in oceanic environments, such as of water temperature and salinity (e.g. Elderfield & Ganssen, 2000). Moreover, improvements in the precision of mass spectrometry measurements have allowed Mg stable isotope systems to be explored (e.g. Young & Galy, 2004). Mg isotopic variations observed in nature, both biological and inorganic, have served as tracers for investigations of a variety of processes, such as chemical weathering of rocks and minerals, material transport among the reservoirs of the Earth system, magmatic processes, and for paleoenvironmental reconstructions (e.g. Galy *et al.*, 2002; Tipper *et al.*, 2006, 2010; Pogge von Strandmann, 2008; Pogge von Strandmann *et al.*, 2008; Hippler *et al.*, 2009; Higgins & Schrag, 2010; Jacobson *et al.*, 2010; Yoshimura *et al.*, 2011).

Mg chemical environments are also of fundamental importance in geologic materials. X-ray absorption near-edge structure (XANES) is one of the best techniques for the determination of the chemical environment of matter, since it

is a molecular-scale analytical technique that yields electronic and structural information about an element of interest (Stöhr, 1992). The XANES spectrum is characterized by resonance excitation of a core electron into unoccupied orbitals. Because core electrons excited by X-ray absorption are localized to the atoms from which they originate, X-ray core-electron transitions allow investigation of the chemical properties of specific elements in complex materials, and provide information about the geometric arrangement of the elements of interest. The spectrum provides constraints for determining phases involved in geochemical reactions (e.g. Wong *et al.*, 1994; Li *et al.*, 1999; Wispelaere *et al.*, 2004; Finch & Allison, 2008; Foster *et al.*, 2008; Ingall *et al.*, 2011). Recently, the application of Mg *K*-edge XANES to characterize the local environment of Mg in biogenic CaCO₃ produced by corals, bivalves and brachiopods has provided direct evidence for Mg incorporation into CaCO₃ (Finch & Allison, 2008; Foster *et al.*, 2008; Cusack *et al.*, 2008). This technique also offers the possibility of examining information on the speciation without any destruction of material.

While recent development of X-ray analytical techniques makes it possible to resolve more detailed features of Mg *K*-edge XANES spectra (e.g. Cusack *et al.*, 2008; Trcera *et al.*, 2009), there have been few systematic studies of Mg *K*-edge XANES data from geologic materials (minerals, rocks, sediments, glass) for use as potential reference spectra (Finch & Allison, 2007; Trcera *et al.*, 2009). To better understand the

[‡] Present address: Japan Agency for Marine-Earth Science and Technology, 2-15 Natsushima-cho, Yokosuka-city, Kanagawa 237-0061, Japan.

Table 1
Materials measured in this study.

Group	Sample name	Formula/material	CN	Crystal structure	Peak 1 (eV)	Peak 2 (eV)	Peak 3 (eV)
Minerals	Calcite	CaCO ₃	6	Trigonal	1309.2	1313.3	1323.4
	Basic magnesite	MgCO ₃ + Mg(OH) ₂			1312.0	1315.1	
	Dolomite	CaMg(CO ₃) ₂	6	Trigonal	1308.3	1313.2	
	Cordierite	Mg ₂ Al ₃ (AlSi ₅ O ₁₈)	6	Orthorhombic	1311.8	1315.4	1325.3
	Garnet	A ₃ B ₂ (SiO ₄) ₃ [A = Ca, Mg, Mn; B = Al, Cr]	8	Cubic	1311.2	1314.6	
	Rhodonite	(Mn,Ca) ₅ Si ₅ O ₁₅		Triclinic	1310.8	1314.4	1318.6
	Amphibole	Na ₂ (Fe,Mg) ₃ Fe ₂ Si ₈ O ₂₂ (OH) ₂	6	Monoclinic/ orthorhombic	1310.9	1314.5	
	Labradorite	(Ca,Na)(Si,Al) ₄ O ₈		Triclinic	1315.0		
	Serpentine #1	(Mg,Fe) ₃ Si ₂ O ₅ (OH) ₄	6	Monoclinic	1310.1	1315.1	
	Serpentine #2	(Mg,Fe) ₃ Si ₂ O ₅ (OH) ₄					
	Olivine	(Mg,Fe) ₂ SiO ₄	6	Orthorhombic	1315.2		
Pickeringite	MgAl ₂ (SO ₄) ₄ ·22H ₂ O	6	Monoclinic	1311.4	1315.6		
Rocks	Unakite	–	–				
Glass	Obsidian	–	–				
Reference materials	GSJ JLk-1	Lake sediment	–	–	1311.0	1314.5	1318.8
	GSJ JA-1	Andesite	–	–	1311.0	1314.8	1319.5
	GSJ JB-2	Basalt	–	–	1310.5	1314.3	1319.0
	GSJ JG-1a	Granodiorite	–	–	1311.0	1314.5	1318.9
	USGS COQ-1	Carbonatite	–	–	1311.0	1314.2	1319.4
	Chemical reagents	Magnesium silicide	Mg ₂ Si	4	Cubic		
Magnesium oxide		MgO	6	Cubic	1309.4	1315.2	1317.8
Magnesium hydroxide		Mg(OH) ₂	6	Hexagonal	1310.2	1314.4	1318.2
Magnesium sulfate		MgSO ₄	6	Orthorhombic	1308.1	1310.4	1315.7
Magnesium sulfate heptahydrate		MgSO ₄ ·7H ₂ O	6	Orthorhombic	1310.6	1315.4	

behavior of Mg in the geochemical environment, we produced a suite of Mg *K*-edge XANES spectra from Mg-bearing silicate and carbonate minerals, sediments, rocks and chemical reagents. The aim of our study was to provide an overview of the spectral features and variations of Mg *K*-edge XANES in geologic materials.

2. Materials and methods

XANES measurements were carried out at the c-branch of the soft X-ray photochemistry beamline (BL27SU) in the SPring-8 facility. The light source was radiation from a figure-8 undulator, which produces a linearly polarized photon beam (Tanaka *et al.*, 1998). The photon beam was dispersed by a soft X-ray monochromator with varied-line-spacing plane gratings (Ohashi *et al.*, 2001). XANES spectra were measured by scanning the undulator gap as well as the monochromator scan to maintain maximum intensity of the incident soft X-rays, and by scanning the width of entrance and exit slits to maintain constant resolving power. The photon energy resolution during the measurements was set at 250 meV. The beam size at the focus point was a ~ 500 μm -diameter circle with a photon flux of 1×10^{11} photons s^{-1} (Tamenori *et al.*, 2007). During XANES measurements, the intensity of the incoming photon beam (I_0) was monitored by measuring the drain current on the surface of a post-focusing mirror.

For XANES measurements, geological samples were powdered to ensure that sample orientation and inhomogeneity did not influence the results. Powdered geologic materials and chemical reagents were fixed with conductive double-sided carbon tape onto a sample holder. The sample

holder was fixed on a linear and rotatable manipulator and installed in a vacuum chamber at a pressure of 1×10^{-5} Pa. Spectra were recorded simultaneously in total electron yield (TEY) by measuring the sample drain current and in partial-fluorescence yield (PFY) by using a silicon drift detector (SDD) (Tamenori *et al.*, 2011). The SDD was mounted perpendicular to the axis of the incident photon beam. Monochromatic light was irradiated at an angle of about 80° to the sample normal to minimize contamination by elastic scattering. The materials measured in this study are listed in Table 1. Some of the materials do not have Mg in the composition formula; this indicates substitution of cation sites by Mg. The selected energy range for Mg XANES measurements was 1300–1350 eV with an energy step of 0.2 eV and an acquisition time of 4 s.

The energy calibration was performed by the following method, and reference data of the energy calibration were obtained. A hemispherical electron analyzer equipped with a gas cell was installed in front of the XANES measurement chamber to determine the absolute excitation photon energy. During XANES data collection for the standard material (MgO), the gas cell was filled with Ne (2×10^{-4} Pa) gas and the photon energy was calibrated by measuring the binding energy of the Ne 1s electron (870.2 eV) at all scanning points. Because energy calibration by this technique requires a long accumulation time, the photon energy scale of another sample was calibrated against the XANES spectrum of MgO.

Data analysis to remove the background and qualitatively analyze the XANES spectra was carried out manually. The data were normalized for variations in the primary X-ray intensity (I_0). A linear pre-edge was removed for each spec-

trum and the data were normalized by the height of the edge-jump. For geologic samples, spectra recorded by PFY exhibited spectral patterns identical to those recorded by the TEY method because concentrations of Mg in the samples were low, and the distortion of spectra by self-absorption effects was negligible. Because the statistics of the PFY data were better than those of the TEY data, the PFY data were used for the following discussion.

3. Results and discussion

3.1. Oxide, sulfate and silicide

Stacked Mg *K*-edge XANES spectra collected from Mg-bearing compounds exhibited several features that varied markedly among the compounds. The variations were more pronounced for photon energies below 1320 eV. The positions of the most intense peaks of the oxides, sulfates and silicides differed (Fig. 1).

The spectrum of periclase (MgO) provides a model for Mg in regular octahedral coordination, and it consists of a lattice of a Mg²⁺ ion and O²⁻ ions. The spectral features we obtained for MgO agree well with those of previous studies (*e.g.* Ildefonse *et al.*, 1995; Aritani *et al.*, 2000), showing pronounced peaks at 1309.5, 1315 and 1318 eV. Smaller peaks were evident at 1311.5 and 1322 eV. We obtained a broad peak at about 1327 eV, which appeared to represent interference of multiple peaks and/or the beginning of the EXAFS oscillations.

The spectra of both magnesium sulfate (MgSO₄) and magnesium sulfate heptahydrate (MgSO₄·7H₂O) showed two pronounced peaks at about 1311 and 1316 eV, with a shoulder at about 1308 eV (Fig. 1). The heights of these peaks were lower for MgSO₄·7H₂O. There were three additional peaks in

the MgSO₄ spectrum, at 1319, 1321 and 1330 eV. The spectrum of another hydrated Mg sulfate [pickeringite; MgAl₂(SO₄)₄·22H₂O] was similar to those of the other two sulfate compounds, but the peak position was at slightly higher energy. The shifts in the pronounced peaks are caused by an alteration of the geometrical and chemical environment of the Mg owing to crystal water of hydrated Mg sulfate groups. The spectral peaks of MgSO₄ were weaker for the hydrated sulfates, which exhibited a smoother spectrum than MgSO₄ (Fig. 1).

Although MgSO₄·7H₂O is thought to partially dehydrate in a vacuum chamber, the differences of the sulfate spectra might reflect changes of the geometric and chemical environment of magnesium related to the presence or absence of crystal water, which has been demonstrated for sulfates of other elements (Kruse *et al.*, 2009; Yoshimura *et al.*, 2013). This feature can also be explained by some degree of disorder or partly amorphous material. The spectral shape of the three sulfate compounds was very similar below 1316 eV, which appears to be a distinguishing feature of sulfate compounds.

The spectrum of magnesium silicide (Mg₂Si), which manifests in the form of two Mg atoms attached by double bonds to a Si atom, showed several distinguishing features (Fig. 1). The main peaks appeared at 1306, 1310, 1315 and 1319 eV, but were much broader and of lower amplitude than those of the other Mg compounds (Fig. 1). The relatively featureless spectrum we obtained for Mg₂Si, having a coordination number of four with respect to Mg (Table 1), implies that post-edge features tend to become more complex with decreasing coordination number (CN). The Mg₂Si peaks were at lower energy levels and had lower amplitudes than those of the other Mg compounds. Ildefonse *et al.* (1995) reported that the first resonance shifts to higher energy as CN increases. Their XANES spectra of MgAl₂O₄ (CN = 4), MgO (CN = 6) and Mg₃Al₂Si₃O₁₂ (CN = 8) showed the energy shift to be ~1 eV between ^[4]Mg and ^[6]Mg, and between ^[6]Mg and ^[8]Mg. It has also been confirmed that coordination changes from ^[4]Mg to ^[8]Mg in oxide and silicate minerals shifts the most intense peak to higher energy positions in the spectra and decreases their amplitudes (Li *et al.*, 1999). Moreover, the XANES spectrum of Mg metal (Wong *et al.*, 1994) has a similar shape to Mg₂Si. Both Mg metal and Mg₂Si peaks are characterized by low amplitudes and these white lines shift to lower energy levels (Fig. 1). The spectral character of the silicide sample might be due to the influence of the oxidation state and may also be influenced by the poor crystallinity of the Mg₂Si.

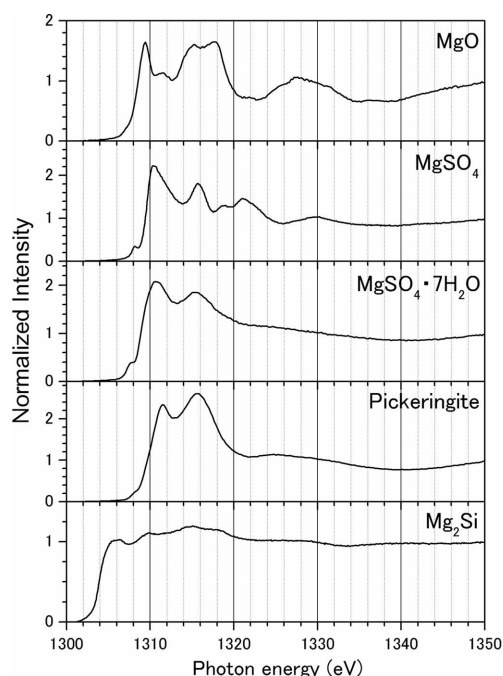


Figure 1
Mg *K*-edge XANES spectra of Mg oxide, Mg sulfates and Mg silicide.

3.2. Carbonate minerals and magnesium hydroxide

The stacked spectra of carbonate minerals (calcite, dolomite and basic magnesite) and magnesium hydroxide are shown in Fig. 2. The most pronounced peaks were at 1313 eV for calcite (CaCO₃) and dolomite [CaMg(CO₃)₂] and at 1312 eV for basic magnesite (MgCO₃). The spectral features of the calcite and dolomite are similar to those previously reported (Finch & Allison, 2007; Cusack *et al.*, 2008). In the calcite spectrum, weak shoulders appeared at lower energy (1309 eV) than the

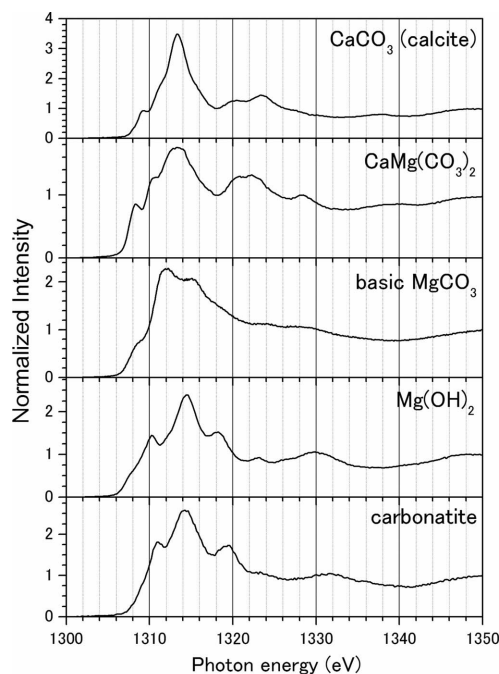


Figure 2
Mg *K*-edge XANES spectra of Mg carbonates, Mg hydroxide and carbonatite.

strongest peak (1313 eV) (Fig. 2). Two similar shoulders in the dolomite spectrum were stronger than those in the calcite spectrum. Moreover, the intensities of the shoulders relative to the main peak at 1313 eV were higher for dolomite. For both calcite and dolomite, some peaks were evident in the post-edge region. The relative heights of those peaks are slightly different from those of Cusack *et al.* (2008). Because substitution of Ca for Mg produces a sub-lattice contraction, and because the Mg–O bond length (2.10 Å) is shorter than the Ca–O bond length (2.36 Å), these variations may reflect compositional heterogeneity (Mg/Ca molar ratios) of diverse double carbonate phases such as dolomite, protodolomite and Ca-dolomite. The relative heights of peaks could also result from experimental settings. For example, larger beam sizes are preferred in order to account for the local heterogeneity of mineral grains.

The overall shapes of the spectra of the Mg(OH)₂ and basic MgCO₃ also agree well with previous studies (*e.g.* Aritani *et al.*, 2000; Finch & Allison, 2008). The spectrum of basic MgCO₃ exhibited a pronounced peak at about 1312 eV with a strong shoulder at about 1315 eV (Fig. 2), but the small peaks at energy levels higher than the main peak were weaker than those of the other carbonate minerals.

Differences of edge peaks of XANES spectra show characteristic differences among Mg compounds. For example, the spectrum of Al₂MgO₄ (data not shown) exhibits an edge peak 2.4 eV lower than that of MgO (Aritani *et al.*, 2000). Al₂MgO₄ has a spinel structure, in which all Mg cations occupy tetrahedral sites. Periclase (MgO) is the model compound for Mg in regular octahedral coordination. The edge energy values of other samples with distorted octahedral structures, Mg(OH)₂ (CdI-type structure) and basic MgCO₃ (mixture of several

types of distorted octahedra), are higher than that of MgO (compare Figs. 1 and 2). The order of increasing edge energy, tetrahedron < octahedron < distorted octahedron, reflects the energy level of Mg 3*p* in a tetrahedron being lower than that in an octahedron, and the energy level of a distorted octahedron becomes higher than that of an octahedron due to broadening and/or splitting of the 3*pσ** state (Aritani *et al.*, 2000). The position of an edge peak can be at lower energy than the main peak when the cation is in a lower coordination state with the same valence.

No peaks associated with carbonate minerals were identified in the carbonatite sample (Fig. 2), indicating that the Mg in the sample is not predominantly in carbonate compounds. The overall spectral character of the carbonatite sample may be affected by the presence of Mg silicate minerals, especially pyroxenes and amphiboles (Fig. 3). The similarity was also found between carbonatite and Mg(OH)₂ (Fig. 2). The only spectral difference was that peaks were slightly shifted to higher energies in the spectrum of carbonatite.

3.3. Silicate minerals

Fig. 3 shows the Mg *K*-edge XANES spectra we obtained for various minerals including the typical rock-forming groups of amphiboles, feldspars (labradorite), pyroxenoids (rhodo-

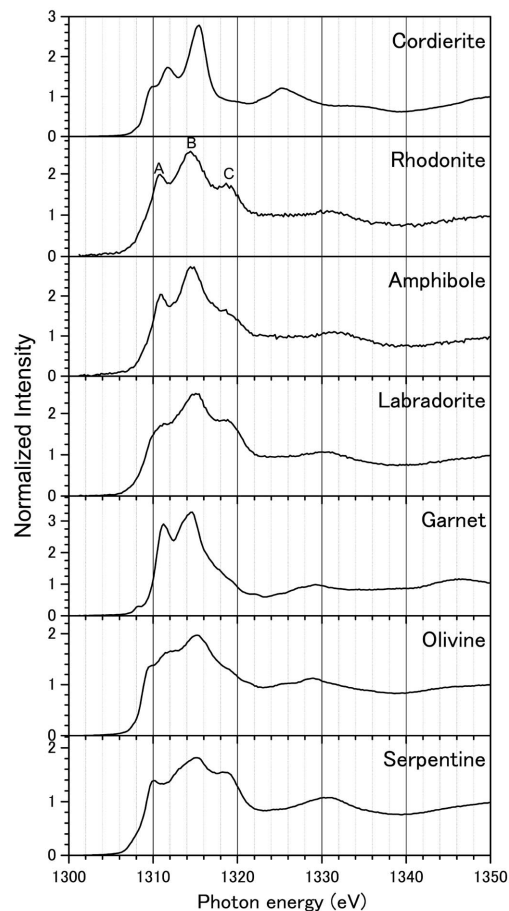


Figure 3
Mg *K*-edge XANES spectra of silicate minerals.

nite) and olivines. There were three prominent features (labeled *A*, *B* and *C* in Fig. 3) in near-edge energy regions (<1320 eV), as in previous studies (Li *et al.*, 1999; Trcera *et al.*, 2009), and a few broad oscillations in the post-edge energy range (>1320 eV). For cordierite [Mg₂Al₃(AlSi₅O₁₈)], there was also a weak pre-edge shoulder at the lower energy side of peak *A* (Fig. 3). For olivines [(Mg,Fe)₂SiO₄] and cordierite, Li *et al.* (1999) noted another peak between peaks *A* and *B*, which may be related to the strong distortion of the first Mg–O coordination shell, in agreement with the calculated spectrum of enstatite (Cabaret *et al.*, 1998).

Wu *et al.* (1996) and Cabaret *et al.* (1998) made quantitative full multiple scattering calculations for the Mg *K*-edges of olivines (forsterite) and pyroxenes (diopside and enstatite), respectively. These studies provided excellent simulations of the experimental spectra, and showed that the most pronounced peak was related to the first coordination shell and may be attributed to the electronic transition of 1s to the empty bound 3p-like state within the first coordination sphere (Wu *et al.*, 1996). It has been proposed that other examples of peaks *A* and *C* and the broad oscillations in the post-edge region are related to multiple scattering from the outermost coordination shell around the absorbing Mg ion (Cabaret *et al.*, 1998). Moreover, the post-edge oscillations may be EXAFS oscillations related to multiple scattering from the first coordination shell and/or single-scattering from the outermost coordination shell. Full EXAFS spectra would have to be analyzed to determine the contributions from these effects.

The cations in pyroxenes are located in the sixfold (*M1*) sites and/or the eightfold (*M2*) sites of the structure (*e.g.* Clark & Papike, 1968). Orthopyroxenes are single-chain silicates with ideal compositions of Mg₂Si₂O₆ (enstatite) and Fe₂Si₂O₆ (ferrosilite), where Mg and Fe substitute for each other in two non-equivalent *M1* and *M2* sites to form a solid-solution series. Experimental Mg *K*-edge XANES spectra of synthetic orthopyroxenes have shown that peak intensities vary as a function of chemical composition along the enstatite–ferrosilite series (Giuli *et al.*, 2002). The height of the peak at 1314.5 eV relative to that at 1319 eV decreases with increasing enstatite content. The variations in relative intensities of the pronounced peaks may reflect compositional variability of the pyroxenes (Giuli *et al.*, 2002).

The XANES spectrum we obtained for rhodonite [(Mn,Ca)₅Si₅O₁₅] shows three peaks in the near-edge region (labeled *A–C* in Fig. 3) and a broad peak in the post-edge region. These features compare well with spectra from synthetic (Ildefonse *et al.*, 1995; Li *et al.*, 1999) and natural diopside (Cabaret *et al.*, 1998; Mottana *et al.*, 1999) and indicate that the arrangement of backscattering atoms surrounding the Mg absorber does not change substantially, although it is classified as a pyroxenoid. The highest peak (*B*) arises from interaction of the photoelectron emitted by Mg with the six nearest-neighbor O atoms in the first coordination shell; it reflects the fundamental atomic properties of the Mg–O interaction and gives an indication of short-range order around Mg at the *M1* site of pyroxenes (Mottana *et al.*,

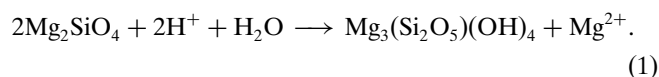
1999). However, the spectrum we obtained for rhodonite contains far fewer features than that of periclase (MgO), which is the model compound where Mg is in regular octahedral coordination (Fig. 1). The pronounced peaks on the rhodonite spectrum at around 1311 and 1319 eV are indicators of medium-range order and provide information about sample crystallinity (Mottana *et al.*, 1999).

A significant change in relative heights of the main peaks has also been observed across the compositional range of clinopyroxenes (Mottana *et al.*, 1999). However, the spectrum of omphacite, Ca–Na clinopyroxene, shows that variations in the relative heights of the peaks are not directly related to sample composition in terms of the ratio of diopside to jadeite (Mottana *et al.*, 1999).

The energy positions of peaks for rhodonite, amphibole, labradorite and garnet were almost identical but their relative intensities varied (Fig. 3). The XANES spectrum of amphibole and labradorite had a similar shape to rhodonite. By contrast the relative intensities of peak *C* decreased in the amphibole and the peaks *A–C* were not well resolved in the spectrum of labradorite (Fig. 3). Peak *C* was not observed in garnet but peaks *A* and *B* remained at almost the same energy position in the other minerals (Fig. 3). Fingerprinting identification may only be possible by relative intensities since these compounds have quite different crystal structures and the energy positions of main peaks were very similar.

Olivine showed a strong peak at 1315 eV, with two shoulders at lower energy, one shoulder at higher energy and a broad peak at 1329 eV (Fig. 3). These features have also been recognized in the theoretical spectrum of forsterite (Wu *et al.*, 1996, 2004; Trcera *et al.*, 2009). It is still being debated whether Mg and Fe in olivines occur in two non-equivalent sites, *M1* or *M2*. Wu *et al.* (2004) presented high-resolution experimental spectra for a synthetic olivine that was the intermediate 1:1 member of the forsterite–fayalite solid solution series. The experimental spectra reproduced in general form their theoretical spectra, although peak widths and relative amplitudes showed substantial disagreement.

Serpentinization of olivine is a common replacement reaction in rocks. If we assume olivine to be forsterite and serpentine to be lizardite, the replacement reaction can be expressed as



Both olivine and serpentine [(Mg,Fe)₃Si₂O₅(OH)₄] have prominent spectral peaks at 1315 eV, but display several differences from the spectra of other minerals and rocks (Fig. 3). Compared with the olivine spectrum, neither of the two serpentine spectra show the peak at about 1311.5 eV in the olivine spectrum; both of them show a peak at 1319 eV that is absent from the olivine spectrum, and the peak at 1329 eV in the olivine spectrum is replaced by a peak at ~1331 eV.

3.4. Sediments, rocks and silicate glass

The near-edge regions of the spectra of three rock standards (JA-1, JB-2 and JG-1a) and a sediment standard (JLk-1) all showed three pronounced peaks at about 1311, 1314 and 1319 eV (A, B and C on Fig. 4). The spectra of these reference materials were very similar, but the relative intensities of the three main peaks of each varied.

JA-1 and JB-2 are classified as augite-hypersthene andesite collected from Quaternary Old Somma Lava, Hakone Volcano, and tholeiitic basalt (augite-bronzite basalt) from the 1950–1951 eruption of Izu-Oshima, respectively (Ando *et al.*, 1987; Imai *et al.*, 1995). Common minerals of these volcanic rocks include amphibole, pyroxene and plagioclase for andesite, and pyroxene, olivine and plagioclase for basalt. The intensities of peaks A–C decreased in the order $B > A > C$ for JA-1 and JB-2. The spectra of standards JA-1 and JB-2 were similar to that of pyroxene, which is a common mineral in both rock types (Fig. 4).

In contrast, the intensity of the peaks for standard JG-1a (biotite granodiorite, Sori granodiorite 85 Ma, Azuma, Gunma) decreased in the order $B > C > A$ (Fig. 4). Common minerals of Sori granodiorite include quartz, plagioclase, perthite and biotite (Ueda, 1956). The most plausible source of Mg is biotite, which has not been measured in this experiment. The spectra of three igneous rock standards show variations in the relative heights of the peaks which relate to Mg-bearing mineral assemblage.

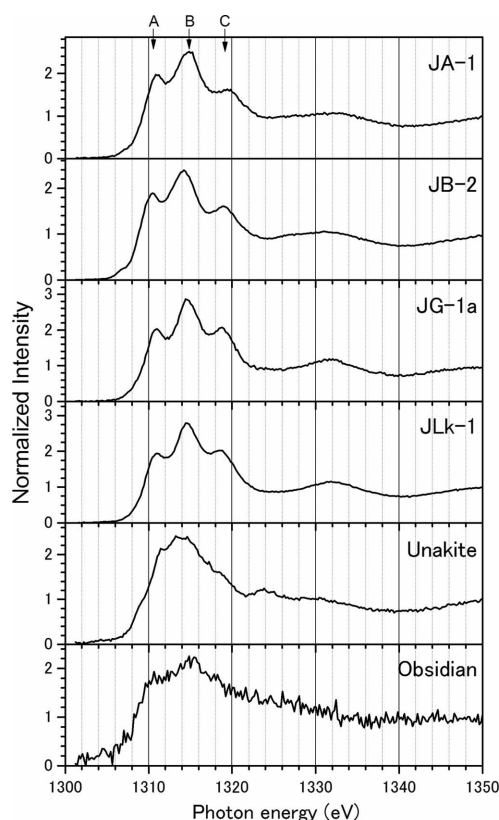


Figure 4
Mg *K*-edge XANES spectra of rocks, sediment and glass.

The argillaceous lake sediment JLk-1, collected from Lake Biwa, shows similar peaks to JG-1a (Fig. 4). The surface sediments of Lake Biwa consist of kaolin, chlorite, vermiculite, montmorillonite, halloysite, hydrohalloysite, quartz, feldspar, mica and amphibole with the clay contents of 12–46% (Hashimoto & Tatekawa, 1974). The complexity of a number of Mg-bearing clay and rock-forming minerals is characterized in this sediment. Experimentally obtained spectra of JLk-1 and JG-1a hamper use of Mg XANES as an indicator of the dominant Mg-bearing phase in candidate minerals, and may be attributable to biotite, even though we have not yet shown a suite of clay mineral spectra.

The spectrum of our unakite sample shows features that suggest it contained both silicate and carbonate minerals (Fig. 4). That is, the sub-peak at 1311 eV matches peaks in the spectra of silicate minerals and the peak at 1324 eV matches a peak observed only in the calcite spectrum (Figs. 2 and 3). Another possible explanation for this peak includes as-yet unmeasured mineral.

Coordination numbers in disordered systems such as glasses can be determined by XANES analysis (Ildefonse *et al.*, 1995). The XANES spectra of diopside glass and diopside crystal show similar peaks, though the main peaks are at lower energy levels in the crystal form (Ildefonse *et al.*, 1995). This difference indicates that Mg CN might have decreased in the glassy phase, although its local environment of formation is unknown. If this is so, the position of the edge peak in glassy materials might be related to the proportions of Mg with different CNs. The relative intensities of peaks are dependent on alkali-element compositions (Trcera *et al.*, 2009), but the peaks were difficult to identify from our spectrum, which may simply reflect low concentrations of Mg. Moreover, the overall shape of the spectrum for obsidian was featureless, which arises either from the variable coordination state of Mg or the highly disordered phase.

4. Conclusions

In this paper we present experimental investigations of Mg *K*-edge XANES analysis of geologic materials. We have shown that Mg *K*-edge XANES is a useful tool for fingerprinting Mg-bearing phases of minerals and rocks and indicating their CNs, thus elucidating aspects of Mg partitioning and stable isotope fractionation during various geochemical reactions. By discerning the dominant Mg-bearing phase in geologic materials, XANES analyses can contribute to refinement of our understanding of geochemical environments and to the reconstruction of past geochemical and geologic events. In addition, micro-XANES is used to identify phases involved in materials as well as mapping chemical species of Mg at high spatial resolution.

We thank Dr Masaharu Tanimizu and Dr Kazuya Nagaishi for providing geologic reference materials. This study was conducted with the approval of the SPring-8 Proposal Review Committee (Proposals 2011B1993, 2011B1202, 2012A1556 and 2012B1714).

References

- Ando, A., Mita, N. & Terashima, S. (1987). *Geostand. Newsl.* **11**, 159–166.
- Aritani, H., Yamada, H., Nishio, T., Shiono, T., Imamura, S., Kudo, M., Hasegawa, S., Tanaka, T. & Yoshida, S. (2000). *J. Phys. Chem. B*, **104**, 10133–10143.
- Cabaret, D., Sainctavit, P., Ildefonso, P. & Flank, A.-M. (1998). *Am. Mineral.* **83**, 300–304.
- Clark, J. R. & Papike, J. J. (1968). *Am. Mineral.* **53**, 840–868.
- Cusack, M., Perezhuerta, A., Janousch, M. & Finch, A. A. (2008). *Chem. Geol.* **257**, 59–64.
- De Wispelaere, S., Cabaret, D., Levelut, C., Rossano, S., Flank, A.-M., Parent, P. & Farges, F. (2004). *Chem. Geol.* **213**, 63–70.
- Elderfield, H. & Ganssen, G. (2000). *Nature (London)*, **405**, 442–445.
- Finch, A. A. & Allison, N. (2007). *Mineral. Mag.* **71**, 539–552.
- Finch, A. A. & Allison, N. (2008). *Geophys. Res. Lett.* **35**, 108704.
- Foster, L., Finch, A., Allison, N., Andersson, C. & Clarke, L. (2008). *Chem. Geol.* **254**, 113–119.
- Galy, A., Bar-Matthews, M., Halicz, L. & O’Nions, R. K. (2002). *Earth Planet. Sci. Lett.* **201**, 105–115.
- Giuli, G., Paris, E., Wu, Z., Mottana, A. & Seifert, F. (2002). *Eur. J. Mineral.* **14**, 429–436.
- Hashimoto, M. & Tatekawa, M. (1974). *Bull. Limnol. Lab. Shiga Univ.* **24**, 74–88.
- Higgins, J. A. & Schrag, D. P. (2010). *Geochim. Cosmochim. Acta*, **74**, 5039–5053.
- Hippler, D., Buhl, D., Witbaard, R., Richter, D. K. & Immenhauser, A. (2009). *Geochim. Cosmochim. Acta*, **73**, 6134–6146.
- Ildefonso, Ph., Calas, G., Flank, A. M. & Lagarde, P. (1995). *Nucl. Instrum. Methods Phys. Res. B*, **97**, 172–175.
- Imai, N., Terashima, S., Itoh, S. & Ando, A. (1995). *Geostand. Newsl.* **19**, 135–213.
- Ingall, E. D., Brandes, J. A., Diaz, J. M., de Jonge, M. D., Paterson, D., McNulty, I., Elliott, W. C. & Northrup, P. (2011). *J. Synchrotron Rad.* **18**, 189–197.
- Jacobson, A. D., Zhang, Z., Lundstrom, C. & Huang, F. (2010). *Earth Planet. Sci. Lett.* **297**, 446–452.
- Kruse, J., Leinweber, P., Eckhardt, K.-U., Godlinski, F., Hu, Y. & Zuin, L. (2009). *J. Synchrotron Rad.* **16**, 247–259.
- Li, D., Peng, M. & Murata, T. (1999). *Can. Mineral.* **37**, 199–206.
- Mottana, A., Murata, T., Marcelli, A., Wu, Z. Y., Cibin, G., Paris, E. & Giuli, G. (1999). *Phys. Chem. Miner.* **27**, 20–33.
- Ohashi, H., Ishiguro, E., Tamenori, Y., Kishimoto, H., Tanaka, M., Irie, M., Tanaka, T. & Ishikawa, T. (2001). *Nucl. Instrum. Methods Phys. Res. A*, **467**, 529–532.
- Pogge von Strandmann, P. A. E. (2008). *Geochem. Geophys. Geosys.* doi 10.1029/2008GC002209.
- Pogge von Strandmann, P. A., Burton, K. W., James, R. H., van Calsteren, P., Gislason, S. R. & Sigfússon, B. (2008). *Earth Planet. Sci. Lett.* **276**, 187–197.
- Stöhr, J. (1992). *NEXAFS Spectroscopy*. Berlin: Springer.
- Tamenori, Y., Morita, M. & Nakamura, T. (2011). *J. Synchrotron Rad.* **18**, 747–752.
- Tamenori, Y., Ohashi, H., Ishiguro, E. & Ishikawa, T. (2007). *Rev. Sci. Instrum.* **78**, 1588–1590.
- Tanaka, T., Maréchal, X.-M., Hara, T., Tanabe, T. & Kitamura, H. (1998). *J. Synchrotron Rad.* **5**, 459–461.
- Tipper, E. T., Gaillardet, J., Louvat, P., Capmas, F. & White, A. F. (2010). *Geochim. Cosmochim. Acta*, **74**, 3883–3896.
- Tipper, E. T., Galy, A., Gaillardet, J., Bickle, M. J., Elderfield, H. & Carder, E. A. (2006). *Earth Planet. Sci. Lett.* **250**, 241–253.
- Trcera, N., Cabaret, D., Rossano, S., Farges, F., Flank, A.-M. & Lagarde, P. (2009). *Phys. Chem. Miner.* **36**, 241–257.
- Ueda, Y. (1956). *J. Mineral. Petrol. Economic Geol.* **40**, 178–184.
- Wong, J., George, G. N., Pickering, I. J., Rek, Z., Rowen, M., Tanaka, T., Via, G. H., DeVries, B., Vaughan, D. E. W. & Brown, G. E. Jr (1994). *Solid State Commun.* **92**, 559–562.
- Wu, Z., Mottana, A., Marcelli, A., Natoli, C. R. & Paris, E. (1996). *Phys. Chem. Miner.* **23**, 193–204.
- Wu, Z., Mottana, A., Marcelli, A., Paris, E., Giuli, G. & Cibin, G. (2004). *Phys. Rev. B*, **69**, 104106.
- Yoshimura, T., Tamenori, Y., Iwasaki, N., Hasegawa, H., Suzuki, A. & Kawahata, H. (2013). *Chem. Geol.*, doi:10.1016/j.chemgeo.2013.05.035.
- Yoshimura, T., Tanimizu, M., Inoue, M., Suzuki, A., Iwasaki, N. & Kawahata, H. (2011). *Anal. Bioanal. Chem.* **401**, 2755–2769.
- Young, E. D. & Galy, A. (2004). *Rev. Mineral. Geochem.* **55**, 197–230.